Synthetic Metals 313 (2025) 117894

Contents lists available at ScienceDirect

Synthetic Metals

journal homepage: www.elsevier.com/locate/synmet

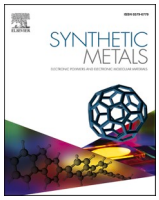

Efficient decoration of graphene oxide with a narrow size distribution of noble metal nanoparticles: Green reduction and integration into a thermoelastic composite

D. Vella [a,*], D. Vengust [b], P. Umek [c], A. Rezaei [a], M. Jezeršek [a], A. Mrzel [b]

[a] Faculty of Mechanical Engineering, Laboratory for Laser Techniques, University of Ljubljana, Aškerčeva 6, Ljubljana 1000, Slovenia
[b] Jožef Stefan Institute, Department of Complex Matter, Jamova 39, Ljubljana 1000, Slovenia
[c] Jožef Stefan Institute, Department of Condensed Matter Physics, Jamova 39, Ljubljana 1000, Slovenia

A B S T R A C T

We have developed a significantly enhanced method for the effective and homogeneous decoration of graphene oxide (GO) and reduced graphene oxide (r-GO) flakes with gold (Au) and platinum (Pt) nanoparticles. This method involves the direct nucleation of nanoparticles on the surface of dispersed GO through a single-step reaction. By carefully controlling the stepwise introduction of gold and platinum complexes at elevated temperatures, without additional reducing agents, we successfully achieved a homogeneous distribution of Au and Pt nanoparticles, ~ 20 nm and ~ 3 nm in size, densely covering the GO sheets. The decoration yield in a mass ratio between Au and GO was up to 20 %. Reduced GO with attached gold and platinum nanoparticles was obtained using ascorbic acid as a reducing agent. Finally, we embedded Au-decorated r-GO in polydimethylsiloxane (PDMS) to form a composite. We show how this stable hybrid material composite can be spin-coated to form a thin thermoelastic film on a flexible substrate, enabling promising photoacoustic properties that could be exploited further in biomedical applications.

1. Introduction

Graphene, graphene oxide (GO), and reduced graphene oxide (r-GO) used as fillers can significantly improve polymer properties [1,2]. Nanocomposites composed of these carbon-based materials exhibit a combination of useful properties such as high electrical conductivity, large surface area, mechanical flexibility, good carrier mobility, thermal conductivity, and transparency in the visible range of the spectrum [3,4]. However, production on a large scale of graphene relies on sophisticated and complex processes that can limit its use in many composite-based applications [5,6]. Small graphene yield in the production volume can be solved by using r-GO, which can be mass-produced by various cost-effective oxidation–reduction methods from graphite [7]. However, GO contains oxygen functional groups that disrupt its sp^2 conjugated backbone, resulting in lower electrical conductivity. Thus, to improve the conductivity, GO must be further converted to r-GO using different approaches such as chemical reduction in water at high pressure and temperature [8], with the use of aluminum powder as a catalyst [9], or very often by hazardous or even toxic reducing agents like $NaBH_4$, hydrazine, and their derivatives [10–12].

In line with the green agenda, synthesis can also be performed using various environmentally friendly reducing agents. These include ascorbic acid [13], glycine [14], reducing sugars [15], and melatonin [16], which have all been used for the preparation of r-GOs from GO. It was shown that combining r-GO with different nanoparticles (NPs), likewise graphene, can significantly improve the light absorbance [17–19] and electrical properties as well [20]. Hybrid systems of this nature showcase significant applications ranging from photoconductive devices [21,22] to electronic devices in biomedical science [23].

Among various attached NPs to the surface of GO, gold and platinum NPs, in particular, have garnered significant attention in recent years due to their interesting properties, including chemical stability, excellent catalytic activity, and biocompatibility [24,25]. The distinctive yellow color of gold originates from its absorption spectrum in the blue and violet parts of the spectrum, primarily due to surface plasmon resonance (SPR). When the size of gold is reduced well below the wavelength of light excitation, a narrower spectral region is absorbed through localized surface plasmon resonance (LSPR). The shape and broadness of the absorbed region heavily depend on particle size and shape [26]. Gold also offers a convenient approach to attaching sulfur-containing groups onto its surface [27,28]. This has attracted considerable attention, and researchers have explored such composite systems in various applications, including electrochemical detectors [29], Surface-Enhanced Raman Scattering Biosensors, chemical

* Corresponding author.
E-mail address: daniele.vella@fs.uni-lj.si (D. Vella).

https://doi.org/10.1016/j.synthmet.2025.117894
Received 1 March 2025; Received in revised form 15 May 2025; Accepted 27 May 2025
Available online 27 May 2025

catalytic applications, and nano-sensors [29–31].

The principal approach to form graphene-Au NPs hybrid nanomaterial is *in situ* technique, involving the formation of NPs in the presence of pristine or functionalized graphene sheets, followed by the direct growth of Au nanostructures onto the surfaces with different reducing, functionalizing, and stabilizing agents. On the other hand, a straightforward path of fabrication GO–Au NPs synthesis is the synchronous reduction of Au metal precursor agents on the surface of non-functionalized GO in a water solution with different reducing agents such as $NaBH_4$, trisodium citrate, and similar [32–34]. *Ex situ* technique comprises the preceding synthesis of NPs and subsequent attachment to the surface of functionalized graphene [35]. For covalent attachment of NPs, the GO is generally more suitable over the r-GO or graphene, due to the vast amount of oxygen functionalities on its surface, which facilitate bonding with other functional groups and better dispersibility. Moreover, dispersing r-GO and especially graphene in aqueous solutions is challenging because of their highly hydrophobic nature [36] and tendency to agglomerate. An alternative solution encompasses the deposition of Au NPs on the GO nanosheets by heating a mixed aqueous solution of $HAuCl_4$ and a GO suspension without a reducing agent. The shapes, sizes, and densities of these NPs varied significantly in terms of the synthesis conditions. Using this method, however, the highest mass ratio $HAuCl_4$ to GO was $3.5 \times 10^{-3,}$ resulting from the densest decoration with Au NPs on the GO surface [37]. The spontaneity of the reaction was determined by the redox potential difference between the different metal precursors and GO, including gold and platinum ions [38].

In this regard, different synthesis methods were also developed for the formation of platinum nanoparticles (Pt NPs) on functionalized graphene, including hydrothermal techniques [39], ethylene glycol (EG) reduction [40], solvothermal methods [41], and microwave synthesis [42]. In particular, such Pt NPs on r-GO form a promising active catalyst for fuel cell applications [43,44].

One of the main advantages of using GO as a building block for the fabrication of hybrid carbon-based materials over its non-oxidized counterpart is its ability to form stable dispersions in several solvents, enabling easy decoration. By exfoliating GO to a single atomic layer, GO sheets exhibit abundant oxygen-containing functional groups (i.e., −OH, −COOH, epoxy groups) on the edges and the surface of GO, which enables easy dispersion even in water [45]. The water solution phase further provides easy and unimpeded access of reactants to the GO surface, opening unlimited avenues for liquid phase processing [46].

Here we report on a straightforward and improved two-step modified bottom-up synthesis decoration method, which is low in cost and toxicity. The method enables easy fabrication of GO or r-GO graphene surfaces with dense and homogenous coverage of surfaces of both materials with Au NPs with diameters between 5 and 40 nm and a mass ratio between Au and GO around 2×10^{-1}. In the first step, Au-decorated GO nanostructures are obtained without the use of a reducing agent. Successively, the reduction of GO to form r-GO-Au nanostructures with remaining initial surface gold decoration was obtained using ascorbic acid as a reducing agent at room temperature. We also used this method to efficiently decorate GO with Pt NPs.

Nanocomposites made of graphene or decorated graphene and polydimethylsiloxane (PDMS) have recently shown great potential as a thermoelastic generator of transient pressure waves, due to the photoacoustic effect [47,48]. Particularly, the transient heating, induced by a short laser pulse, in the filler of the composite causes a rapid change in the volume of the surrounding polymer and the generation of high-frequency and high-pressure waves. This is a tremendous interest in exploring alternative methods in biomedical and clinical procedures, ranging from drug delivery to tumor priming, and high-resolution imaging systems [49–52]. As a proof of concept in the final part of this work, we demonstrate the possibility of obtaining a uniform dispersion of r-GO nanostructures into a PDMS matrix [53]. We show the fabrication of a composite made of PDMS and r-GO decorated with Au NPs, potentially suitable for producing thermoelastic polymers devoted to biomedical applications.

2. Material and methods

GO powder, produced by modified Hummer's method (C/O atomic ratio 1.67), was purchased from ACS Material (Chemical Abstracts Service number: 7782–42–5). The composition in wt% was 51.26 and 40.78 for C and O, respectively. Gold (III) chloride trihydrate ($HAuCl_4$. 3 H_2O, 99.9 %) and L ascorbic acid (99 %) were obtained from Sigma Aldrich chemicals, and K_2PtCl_4 from Alfa Easer. Sylgard 184 silicon elastomer base was purchased from DOW EUROPE GmbH. Other chemicals were of at least analytical reagent grade and used without further purification. Deionized water was used for cleaning apparatus, and the solution was purified with the Millipore system. The distribution of Au and Pt NPs on GO was determined using scanning (SEM-FEI Verios G4, Thermo Fischer) and transmission electron microscopes (TEM, Jeol 2100). The amount of Au and Pt was determined from energy dispersive X-ray data (EDX) measured with an Oxford Instruments Ultim Max SDD 65 mm^2 energy dispersive X-ray (EDX) spectrometer. A transmission electron microscope was used for crystallographic information and characterization of the size of Au and Pt NPs. Distributions in particle size were obtained by evaluating at least 100 NPs per sample. The images were acquired with a Gatan CCD camera Orius. For SEM and TEM analysis, dry materials were dispersed in EtOH using an ultrasonic bath, and then a drop of the dispersion was deposited on the polished surface of an Al sample holder (SEM) and a lacy carbon film supported by a copper grid (TEM). Raman spectra were measured from dry samples using an NT-MDT Spectra assembly, with 488 nm excitation light at a power of 1 mW. The spectra were acquired over 1 minute by integrating consecutive 0.5 seconds acquisition intervals. For accurate measurement of the D and G band positions, a high-resolution grating was used in the region between 1000 and 2000 cm^{-1} , with a resolution of 0.5 cm^{-1} . UV–Vis absorption spectra were recorded using a Cary spectrophotometer by measuring transmission at individual wavelengths with a resolution of 1 nm. For the UV-Vis measurements, a small amount of dried sample was dispersed in water, and spectra were recorded in quartz cuvettes at room temperature.

Fourier transform infrared (FTIR) spectra of selected samples were collected with a PerkinElmer Spectrum 400 Series spectrometer equipped with a universal attenuated total reflection accessory at a resolution of 2 cm^{-1} and an average of 16 scans. The results are discussed in Section 1 of the Suppl. information.

In a typical experiment for gold decoration, 6 mg of GO was dispersed in 100 mL of deionized water using mild ultrasound agitation for 30 minutes. A stable GO dispersion was then heated using an oil bath to 85 °C and kept constant during the decoration procedure. $HAuCl_4$ solution, prepared by dissolving 3 mg of $HAuCl_4$ in 20 mL of deionized water, was added dropwise to the dispersion of GO in deionized water for 40 minutes under vigorous stirring. Dispersing small amounts of $HAuCl_4$ into GO dispersion sequentially through drop-wise addition allow to keep the concentration of that $HAuCl_4$ low throughout the reaction, even though we ultimately add a large amount of it. The reaction mixture was kept at 85 °C for an additional hour and then cooled down to room temperature. The basic procedure for platinum decoration was similar to that for gold; 30 mg of GO was dispersed into 50 mL of deionized water, and a solution of 20 mg K_2PtCl_4 dissolved in 20 mL of deionized water was added dropwise for 40 minutes under stirring and heating. The products were labelled GO-Au and GO-Pt.

For comparison, gold decoration of GO was also prepared with direct heating of prior-prepared GO dispersion in $HAuCl_4$ solution instead of drop-wise addition of the complex to the dispersion of GO. The masses of the reagents and the volume of water remained the same as in the first experiment. Therefore, 6 mg of GO was dispersed in 120 mL of deionized water, and in this dispersion, 3 mg of $HAuCl_4$ was dissolved. The obtained dispersion under vigorous stirring was heated at 85 °C for an hour and then cooled down as in the first experiment.

The resulting GO-Au and GO-Pt flakes were collected by centrifugation at 2500 *rpm*, rinsed three times with water to remove residue of unreacted complex and once with ethanol, and finally dried at 50 °C in an oven. The obtained GO-Au and GO-Pt flakes were dispersible in several solvents, including water, ethanol, or chloroform.

Both r-GO-Au and r-GO-Pt were obtained from GO-Au and GO-Pt using ascorbic acid as a reducing agent, in a subsequent step. 15 mg of starting decorated GO and 110 mg of ascorbic acid were dispersed in 100 mL of deionized water and stirred for 48 hours at room temperature. The precipitated black material r-GO-Au and r-GO-Pt composites were collected by centrifugation, washed several times with deionized water and ethanol, and finally dried at 40 °C in an oven. R-GO-Au material was also used as a filler to demonstrate the fabrication of r-GO-Au / PDMS composite.

Recently, a protocol using simultaneous ultrasound agitation in hexane and vacuum was developed [47]. For the preparation of a PDMS polymer film, 5 mg of r-GO-Au composites nanoflakes in a powder form were added to 5 mL of chloroform and dispersed using soft sonication for 20 min. In a separate vial, we mixed mechanically 1 g of PDMS (Sylgard 184) and 1 mL of chloroform. Then, the obtained mixture was transferred into the vial with r-GO-Au dispersed in chloroform (3 mL), as an initial dispersion. After manual mixing, the final r-GO-Au / PDMS mix was transferred to the ampoule of the rotary evaporator. The total composite made of r-GO-Au, 1 g PDMS, and chloroform 3 mL was continuously mixed in the rotary evaporator, keeping the vacuum with a water pump and soft sonication in a bath Elmasonic P30H (power level 40, frequency 80 kHz). The temperature of the bath was kept below 30 °C by adding ice to the ultrasonic bath. The evaporation/sonication process took around 3 h, and then a cross-linking agent or curing agent was added in the ratio of 1:10 followed by 30 min of stirring. The composite was then spin-coated at 3 krpm velocities on the PDMS substrate. After allocating the samples in the vacuum bell (10^{-3} mbar) for 40 min, they were cured at 80 °C for 1 h, resulting in a PDMS polymer film to obtain well-dispersed graphene in the PDMS polymer matrix, without the need for surface functionalization.

3. Results and discussion

3.1. Optical and structural characterizations

The formation of GO, its decorated derivatives, and derivatives after the reduction of GO with ascorbic acid were first analyzed by UV–vis spectroscopy. Fig. 1a shows the UV-Vis absorption spectra of water-dispersed GO, GO decorated with Au and Pt NPs, and their reduced counterparts. The initial dispersion of GO shows an absorption maximum at 230 nm because of the $\pi \rightarrow \pi^*$ transition involving C = C bonds, and an absorption peak at ~300 nm due to the $n \rightarrow \pi^*$ transition of the C = O bonds. Absorption centered at around 230 nm is present in all GO derivatives. When adding a solution of the gold complex to a GO dispersion dropwise, the formation of Au NPs can be traced as a change in color from yellow to reddish, which persists after redispersing the isolated material. Such color transitions are characteristic of changes that occur in the oxidation state of gold ions and their further agglomeration into Au NPs [54]. An additional optical absorption peak was observed at 525 nm. This is typically assigned to the plasmon resonance of Au NPs. Njoki et al. [54] have also shown that the wavelength of the surface-plasmon absorption band depends on the particle size and the maximum absorption wavelength (λ_{max}) increases with increasing

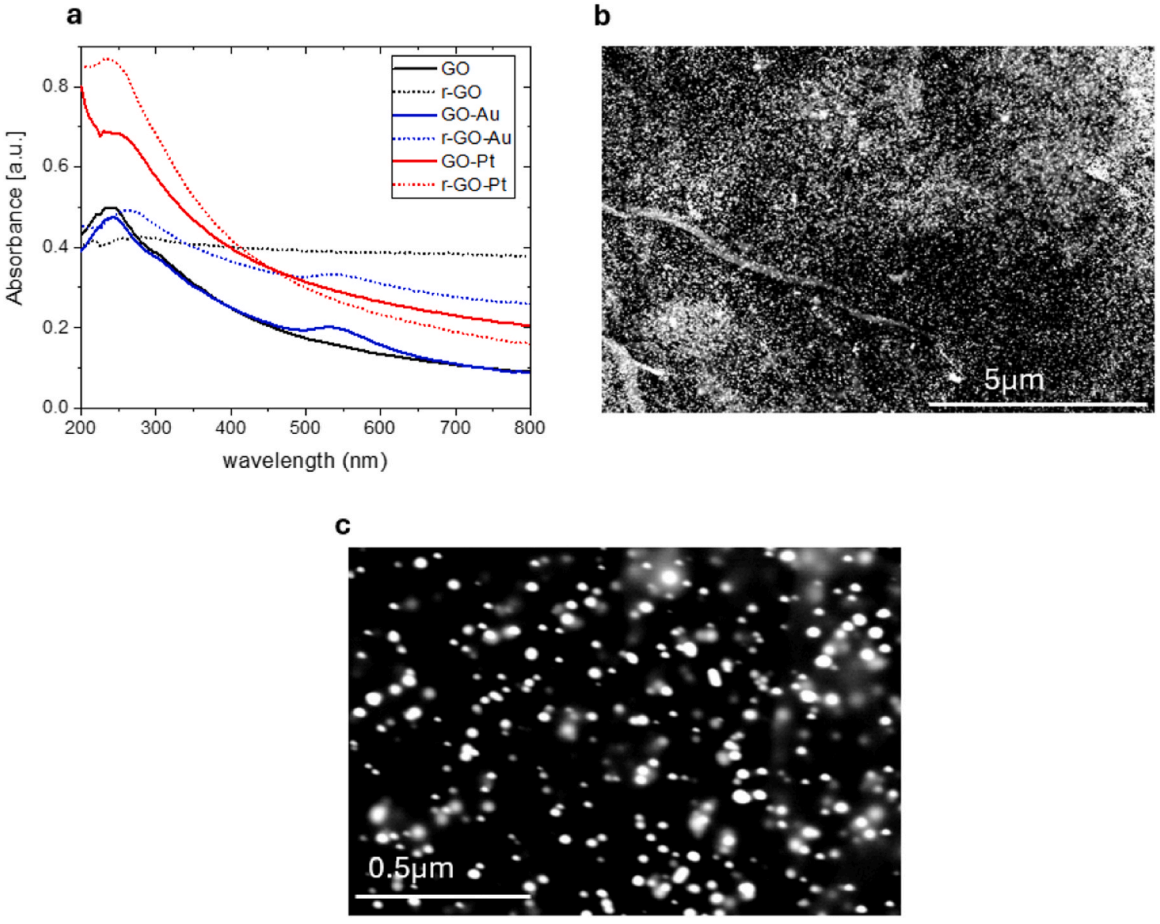

Fig. 1. (a) Absorbance spectra of GO, r-GO, and their decoration with Au and Pt NPs in ethanol dispersion. (b) SEM images of GO-Au over an area of ~ 156 µm^2. Bright spots indicate that GO is fully decorated with NPs (c) A high magnification image displaying the gold NPs distribution over the GO.

diameter: from 519 nm for a diameter of around 20 nm to 569 nm for particles with a diameter of around 100 nm. The dependence can be described by a cubic polynomial curve fitting of the particles diameter (x) as a function of λ_{max}, $\lambda = \lambda_0 + ax + bx^2 + cx^3$ ($y_0 = 518.8$, a = - 0.0172, b = 0.0063, and c = - 0.0000134), yielding the average particle diameter in our samples of around 28 nm (for $\lambda_{max} = 525$ nm). This is further elaborated and more accurately determined with SEM, see Fig. 1b, and TEM (Fig. 2a). The color of the dispersion after the addition of the platinum complex remained practically unchanged, however, the functional dependence of the absorption changed dramatically, indicating possible differences in the UV regions. Gharibshahi and Saion [55] have shown how Pt NPs with an average size in the range from 3.4 to 5.3 nm absorb light in the UV range with two absorption peaks centered at about 216 and 264 nm which shifted to lower wavelengths with decreasing particle size. Additional absorption of graphene species in this region hindered the possible deconvolution of platinum plasmon resonances.

After the reduction, we observed the red shift of the absorbance peak at 230 nm in GO towards 270 nm (r-GO). This peak can be correlated to the electronic transition and is characteristic of r-GO [56]. Pristine r-GO also exhibits a nearly constant absorption throughout the measured wavelength region, similar to a monolayer of graphene. A similar redshift from 230 nm toward 270 nm was also observed in r-GO-Au and r-GO-Pt samples. In the case of GO decorated with platinum, a partial shift of absorption to higher wavelengths is observed due to the electronic transition of GO, meanwhile, the absorbance bands that could be associated with Pt NPs remain.

The sample was subjected to further analysis using SEM. After the decoration with Au NPs, the surface of GO samples consists of round fragments, which can be associated with noble metals. This is confirmed by the compositional image shown in Fig. 1b, c, which show NPs coverage on a large area. The samples treated with gold exhibit homogeneous coverage, with the Au NPs visibly having a bigger diameter than the Pt NPs. Images in Fig. 1b clearly show homogeneous decoration, but to further investigate the materials' crystallinity of Au and Pt NPs and determine the particle size distribution, TEM analysis was performed.

TEM and HRTEM images of the obtained GO-Au materials are shown in Fig. 2a and Fig. 3. The Au NPs of similar sizes densely and relatively uniformly cover the surface of GO sheets. The absence of chlorine in the

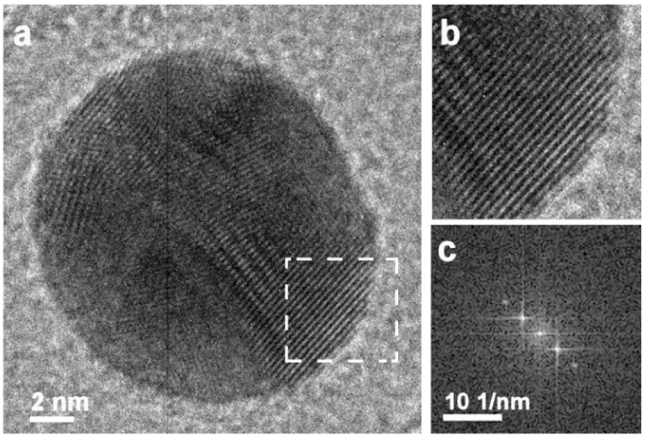

Fig. 3. (a) TEM image of spherical polycrystalline Au NP. (b) HRTEM of the marked area in the image (a), and (c) the corresponding FFT pattern.

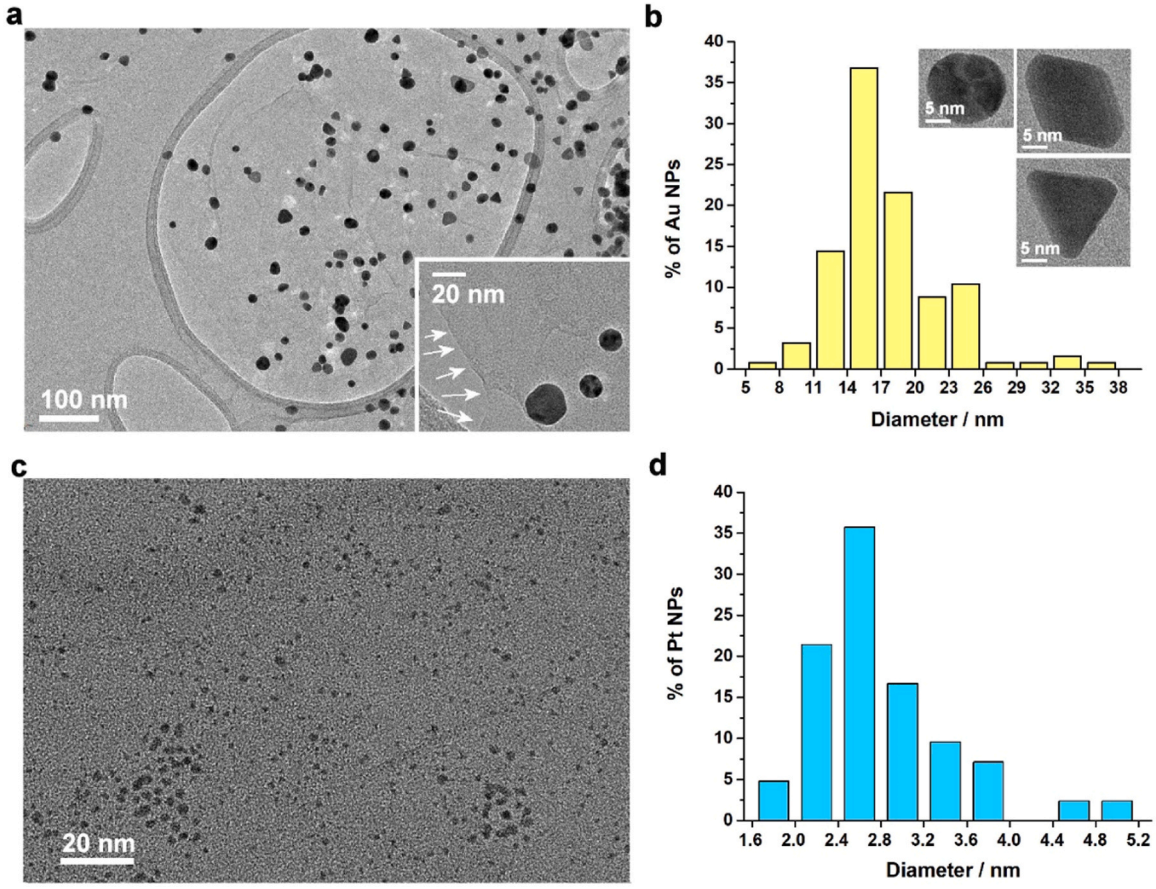

Fig. 2. TEM images of Au (a) and Pt (c) NPs formed on the surface of GO with corresponding Au and Pt NPs size distribution (b, d), respectively. Arrows in the inset to Fig. a are pointing to the edge of the GO sheet. The inset in Fig. b shows Au NPs of different shapes: circular, triangular, and rectangular.

EDS analysis corroborates the reduction of $HAuCl_4$ by GO. Au crystalline/polycrystalline NPs are found to have mainly round morphology; however, some particles have triangular or rectangular shapes (inset to Fig. 2b). A precise size measurement was obtained from TEM images. More than a hundred spherical NPs were measured, and the obtained particle size distributions are shown in Fig. 2b. These particles have diameters between 5 and 38 nm, while more than 50 % of NPs have diameters between 14 and 20 nm. Fig. 3 shows the HRTEM image of an Au nanoparticle with an average diameter of 17 nm, and its interplanar distances. The as-marked distance is 0.26 nm, the value is enlarged and corresponds to the (111) crystal plane face-center cubic Au. The chemical composition of the gold-decorated sample was examined by EDX-TEM (see Suppl. Information Fig. S2a). The amount of Au in graphene is estimated to be around 20 wt% and was determined from EDX-SEM spectra over a larger area.

It is important to emphasize that the mass ratio between $HAuCl_4$ and GO used was 2×10^{-1} and that all the amount reacted with GO, leading to an efficient nucleation of NPs without using additional reducing agents and dropwise control of the complex. This was corroborated by the UV–vis spectra that showed the absence of gold complex in the supernatant dispersion after the isolation of the flakes. In a similar reaction, without a reducing agent, the effective ratio of reacted $HAuCl_4$ to GO ranged from 0.66×10^{-3} to 3.5×10^{-3}, more than an order of magnitude lower [37]. Different types of synthesis where much more mass of gold was used, by directly mixing preformed nanoparticles with GO [29], did not elucidate the amount of Au NPs on the GO surface, and the efficiency of the functionalization. Direct nucleation assisted by reducing agent sodium citrate was also performed in a more complex reflux synthesis, with an initial mass ratio of $HAuCl_4$/GO two orders of magnitude lower [34]. Generally, coverage with NPs was presented in a relatively small area depicted by TEM and atomic force microscopy images, or poorly resolved SEM images. Here, we show homogeneous nucleation of NPs over an investigated area of $\sim 156\ \mu m^2$ in the SEM analysis. The excellent dispersibility of GO in water enables efficient decoration of the flakes, since its reduced counterpart is less dispersible in water solutions.

We found that the method used to add the gold precursor solution to the GO dispersion significantly affects the size of the Au NPs formed. When the Au precursor solution is added dropwise to the GO dispersion, the resulting Au NPs are smaller (Fig. 2a) compared to when the solution is added all at once (see Fig. 4). In the latter case, the Au particles are larger and spontaneously agglomerate into clusters.

Adding small amounts of $HAuCl_4$ into the GO dispersion sequentially through drop-wise addition, under constant agitation/mixing, allows the $HAuCl_4$ concentration to be kept low throughout the reaction. This results in efficient decoration of graphene oxide with a narrow particle size and homogeneous distribution of NPs.

The TEM image of GO decorated with Pt NPs is shown in Fig. 2c, which reveals a dense coverage of the GO surface with Pt NPs. The sample consists of an even coverage of extremely small particles, none bigger than 5 nm. This is also the reason why we couldn't observe any noticeable bright spots with SEM using a backscattered detector. The HRTEM image of Pt NPs formed on the surface of GO is shown in Fig. S1. The chemical composition of the NPs was examined by EDX, confirming the presence of platinum by the characteristic peak at 2.05 keV and several peaks around 9.4 and 11 keV (see Suppl. Information Fig. S2b). The EDX spectrum confirms the presence of platinum. The marked peaks belong to platinum and Cu. The presence of Cu is due to the copper grid in the measurements

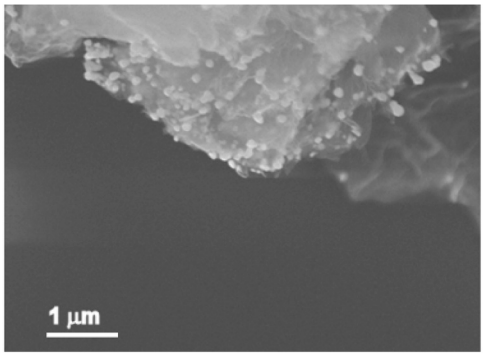

Fig. 4. SEM image of GO decorated with Au NPs. The material was obtained by directly mixing the dispersion of GO in ethanol and the solution of gold precursor.

Platinum particle size distribution in the GO-Pt material is shown in Fig. 2d. To determine the average particle size, several different flakes were analyzed and approximately 100 particle diameters were measured. The high-resolution image and the histogram clearly show that the particle size distribution is small, with all the particles appearing similar in shape and size and the decoration appears to be relatively homogeneous. Pt NPs are much smaller than Au NPs, with average particles having a diameter between 2.0 nm and 3.2 nm. The TEM image does not show any unsupported Pt NPs on the carbon grid, confirming that the nanoparticles are robustly attached to the surface of GO nanosheets.

Multiple factors can contribute to the difference in decoration with Au and Pt. For instance, redox reaction between GO and $PtCl_4^{2-}$ or $AuCl_4^-$ is similar to the spontaneous metal nanoparticle formation on SWNT sidewalls or MoSI nanowires when nanotubes/nanowires are immersed in corresponding noble metal complex solutions [57,58]. Although the surfaces of these nanostructures are chemically very different, the resulting platinum nanoparticles deposited on the surface are significantly smaller than gold nanoparticles. A similar result was observed on the surface of Tungsten oxide nanostructures functionalized with gold or platinum NPs [59]. The author reports that the reduced size of Pt NPs compared to Au NPs may be explained first by the presence of oxidation at the surface of the Pt NPs. Therefore, Pt NPs may have enhanced interaction with the tungsten oxide surface compared to Au NPs due to the presence of an oxide shell; the absence of Au oxidation provides higher mobility and hence increased particle size. On the surface of graphene oxide, we have many groups that contain oxygen, so this could be one of the reasons for the smaller diameters of platinum NPs. In addition, it has been suggested that potential residual chloride contained in the metal complex could also cause increased particle size for gold NPs, due to the high affinity of gold for chlorine [59].

The nucleation reaction involves a galvanic-reaction-like process in which the reduction of $HAuCl_4$ and $PtCl_4^{2-}$occurs on nuclei by the electrons transferred from GO, with accompanying oxidation of GO. For a spontaneous redox reaction, the redox potential of the cathodic reaction should be higher than that of the anodic reaction. The driving force for Au and Pt nanoparticles deposition could be caused by the difference between the reduction potential of $AuCl_4^-$ (0.761 V vs SCE) and $PtCl_4^{2-}$ (0.513 V vs SCE) vs the oxidation potential of GO (0.48 V vs SCE). The proposed redox reaction between GO and $PtCl_4^{2-}$ or $AuCl_4^-$ is similar to the spontaneous metal nanoparticle formation on single-walled nanotubes' (SWNT) sidewalls when nanotubes are immersed in corresponding metal salt solutions. The relative potential levels rationalize the spontaneous electron transfer from the nanotube (oxidation) to the metal ions and their reduction [57].

Based on the reported XPS measurements, a well-accepted mechanism of formation of nanoparticles and the role of the functional groups in GO was proposed. XPS was used to investigate the changes in the GO during the described reactions to determine the mechanism of nanoparticle formation. The data clearly showed that the oxygenated functional groups on the GO surface may play an important part in the formation of noble metal nanoparticles. After the reaction, the peaks associated with C-C bonds (around 284.6 eV) became predominant while the additional peak of C-O (around 286.6 eV) was reduced. These results indicate that the oxygen-containing functional groups on the

surface of GO may be involved in the reduction of noble metal cations to form noble metal nanoparticles. At the same time, these groups are proposed to be the origin of a strong anchoring effect between the noble metal nuclei and the GO surface [37,38,60,61].

The Fourier transform infrared spectra (Fig. S3), shown and discussed in detail in Section 1 of the Suppl. information, are in line with the XPS experimental findings, corroborating the role of the oxygen-containing functional groups during the reduction of the metal complex. Indeed, after the formation of NPs on the GO surface at the expense of the complex, the intensity of the OH band (hydroxyl groups) and the C-O peaks (epoxy and alkoxy groups) [13,62,63] at around 1400 cm^{-1} and 1100 cm^{-1} reduces.

Raman spectra of Graphene Oxide (GO) and its reduced counterparts have been extensively studied. Typically, in the spectra of GO powders, two prominent first-order bands can be distinguished. The G band, located at approximately 1591 cm^{-1} , corresponds to the E_{2g} phonon of sp^2 carbon atoms, and it is characteristic of graphite and graphene [64,65]. In distorted graphite-like phases, the otherwise forbidden D band, observed at 1369 cm^{-1} , becomes clearly resolved [66,67]. This band corresponds to the breathing mode of k-point phonons with A_{1g} symmetry (Fig. 5a). At the double resonance, there are second-order Raman modes, but they are more difficult to resolve in powders and at higher oxidation levels [66].

The intensity ratio of the main D and G bands is commonly associated with the presence and density of defects. Further studies revealed noticeable shifts in these bands and led to the identification of several sub-modes, all linked to structural defects and related to the oxidation states. The D* mode, located just before the main D peak, is associated with edge distortions [68]. Meanwhile, the D″ peak, which appears between the main D and G bands, has been attributed to various distorted bound states. Among these, the presence of amorphous species is believed to play an important role in the increased intensity of this mode [67,69]. Lastly, the D′ mode, found on the higher-frequency side of the main G band, is typically ascribed to disorder-induced phonon modes, and it is particularly well-resolved in larger graphite crystals [70] and thus less important in the study of thin flakes.

Several spectra were recorded across the samples, and Lorentzian fits were applied to extract the positions, widths, and intensities of the two main Raman modes. Pristine GO displays a D/G peak intensity ratio of approximately 0.86, which indicates the presence of disorder arising from vacancies, grain boundaries [57,58] and amorphous carbon species. [59] After reducing GO with ascorbic acid for 24 hours, this ratio increases to an average value of 1.1, indicating a relative growth of the D peak (Fig. 5b). This behavior is not typical for the reduction process [60] but could be ascribed to the increase of the D* , hence to an increase of the edge distortion during the synthesis. Additionally, both the D and G bands shift by more than 10 cm^{-1} toward lower wavenumbers (Fig. 5c, d). While the G band shift can be explained by a characteristic downshift of the D″ mode, commonly seen with reduced oxygen content [67], the D* band is expected to shift in the opposite direction, which leads to an apparent downshift of the prominent D band.

By adding noble metal complexes to the graphene oxide dispersion,

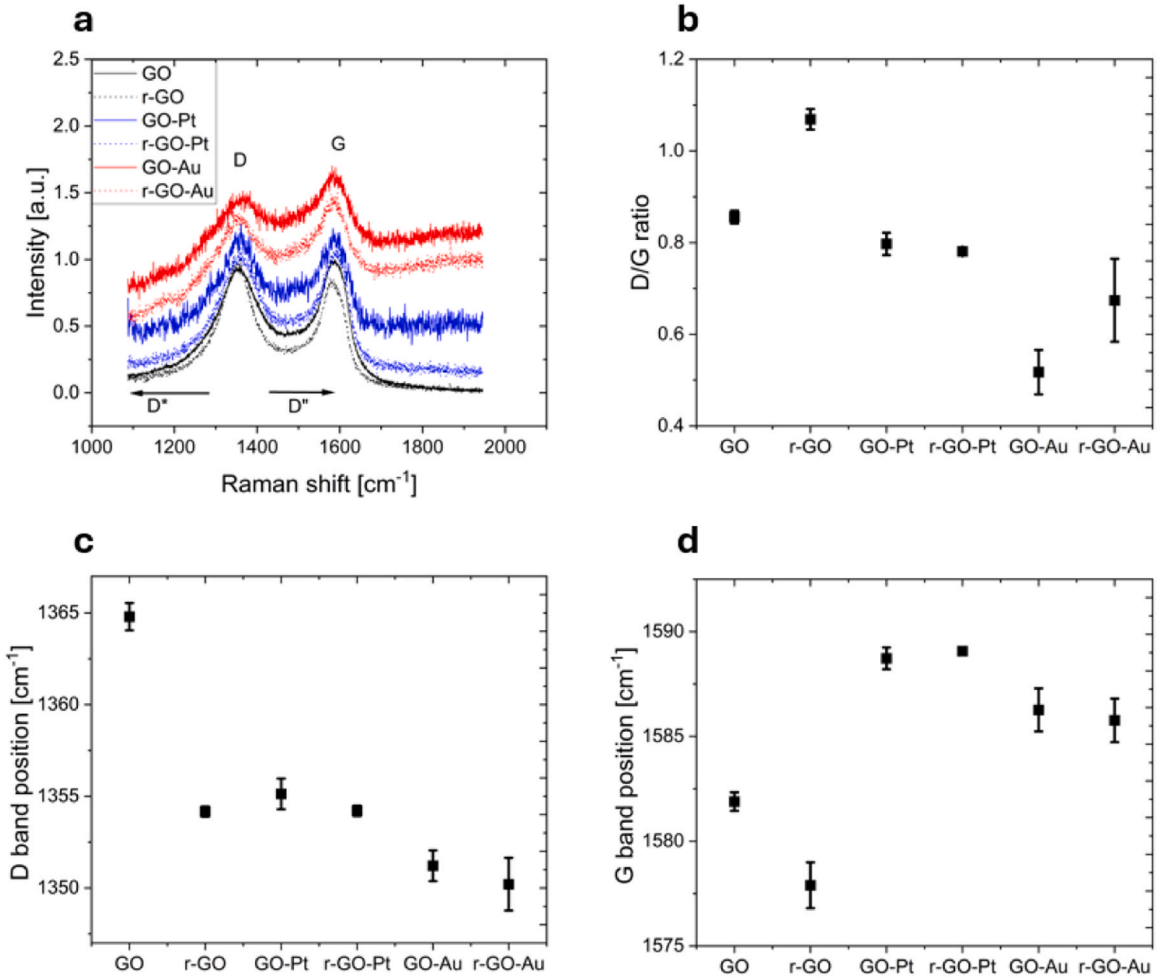

Fig. 5. Raman spectrum of the analyzed samples. (a) Subtracted spectra of the analyzed samples with band positions and possible position (straight line) of additional defect bands D* and D", arrows indicate their displacement upon increasing oxidation level. (b) Values of the corresponding D/G intensity ratio (peak height). D and G band position (cm^{-1}) in (c) and (d) respectively.

the D/G peak intensity ratio drops significantly to 0.5 for the GO-Au composite and only slightly to 0.80 for the GO-Pt composite. This trend is typical for the reduction of pure GO, without many structural defects, and highlights the GO oxidation at the expense of the gold and platinum complex reduction. In the decorated GO the peak position of the D modes red-shifts by 10 cm^{-1} for the Pt-covered sample and 15 cm^{-1} for the Au-covered sample (Fig. 5c). The other G mode shifts to higher energies in both samples. A similar trend has been reported in the thermal reduction process of GO [67], where the shift of the D* mode is toward lower energies as the oxidation level rises, along with a shift of the intermediate D″ mode toward higher energies. The separation of those two peaks impacts the intensity of both main D and G peaks, leading to a relative decrease of the D peak and an increasing intensity of the G peak. For illustrative purposes, the displacement of these sub-modes is indicated in Fig. 5a. After the reduction process, Raman spectra of the platinum- and gold-decorated samples remain largely unchanged. The slight increase in the D/G ratio for the gold sample and the slight decrease for the platinum sample fall within the measurement's standard deviation (Fig. 5b). Other spectral changes are even less pronounced, indicating that the structural alterations in the decorated graphene layers during reduction are minimal compared to those in the reduction of pristine GO.

3.2. r-GO-AuNPs / PDMS composites

R-GO with densely attached noble metal NPs is expected to exhibit a very interesting and promising thermoelastic response as a freestanding film in photoacoustic lensing. However, the primary obstacle in fabricating thin films of these composites using an otherwise highly efficient patented method is the extremely low dispersibility of r-GO and its derivatives in hexane [47]. Solvents that could be used instead of hexane should meet some conditions, such as a relatively low boiling point, the ability to form a dispersion of decorated r-GO derivatives, and the swelling of very viscous PDMS [71].

In this case, PDMS will absorb the solvents through microchannels, and the polymer will gradually saturate with the solvent over time. By checking many suitable common organic solvents that meet all requirements, we have found that at least methyl ethyl ketone with boiling point (bp) 79 °C, chloroform with bp 61 °C, and THF with bp 61 °C could be potentially used as a solvent. First, all of these solvents have similar boiling points to hexane (bp 69 °C). These solvents also enable relatively good dispersability of r-GO obtained by reducing agent ascorbic acid, with stable dispersions for THF and chloroform of around 1.44 μg/mL and 4.6 μg/mL, respectively [72]. The reduction with ascorbic acid does not introduce a level of toxicity like in the case of hydrazine.

The dispersion behavior of chemically r-GO and decorated with gold NPs has been investigated in these solvents, and we found that the most stable dispersion was obtained in chloroform. Together with the combination of its low boiling point and even better-reported compatibility of PDMS in comparison to hexane, chloroform was an obvious choice to fabricate a composite thin film of r-GO-Au and PDMS.

The reduction state of semiconducting GO decreases the electronic bandgap and increases the number of electronic levels available for optical transitions. Particularly, in r-GO, the increasing absorption and thermal conductivity are relevant in optically excited thermoelastic composites [73]. We chose the r-GO-Au as a nanoabsorber since the presence of the nucleated gold nanoparticles further increases the thermal interface in contact with the PDMS for the volumetric expansion, that is, the expander counterpart of the composite. In our previous work [48], we decorated graphene with gold nanoparticles and redispersed it in PDMS and hexane. The dimension of the Au-NPs of around 30 nm effectively increases the thermal interface if compared with the 2–5 nm size platinum NPs, as experimentally and theoretically shown in [48]. However, the nucleation sites of gold nanoparticles were confined to the dangling bonds, or point defects, in the graphene layers. By using GO as a starting material, we obtain a nearly homogeneous spatial distribution of the gold nanoparticles due to the presence of the oxygen functional groups. Moreover, the presence of Au NPs on the GO, likewise in graphene, hinders the restacking of the flakes and facilitates the inter-flakes penetration of the polymers to form a more homogenous composite layer.

In a typical experimental configuration, the dispersion of r-GO-Au (5 mg) into the PDMS matrix (1 g) was obtained by using a method based on continuous sonication-agitation in a vacuum, as reported also elsewhere [47,48]. The dispersion was then spin-coated on a flexible substrate of bare PDMS. To detect the photoacoustic response, the film was irradiated with a nanosecond laser pulse (12 ns) and a laser fluence of 60 mJ/cm^2 in water. This energy density guarantees the operation of this PA emitter in a thermoelastic regime. In this regime, the fraction of light absorbed by the r-GO-Au absorber is quickly transferred to the PDMS matrix, which undergoes transient expansion and contraction. Consequently, a PA wave is launched in the medium (water) and detected by a needle hydrophone. Fig. 6a shows the absorbance of the 17-μm-thick film of r-GO-Au / PDMS that preserves the gold plasmonic resonance peak. The pressure wave signal originates from the thermoelastic film immersed in water upon photoexcitation. The optical absorbance at the 1064 nm laser wavelength excitation is around 0.07 (15 % fraction of absorbed light). Fig. 6b shows the pressure wave signal, typically characterized by a more compressive portion, positive pressure around 800 kPa, and a less prominent negative peak. The propagating planar wave detected by a 30 MHz hydrophone needle (4.5 mm from the source) is captured in shadow photography and shown in Fig. 6b. Within the limitations of the hydrophone and the acoustic attenuation in water, the achievable bandwidth at −6 dB and −20 dB was around 25 MHz and 40 MHz respectively (Fig. 6c) while the optical-to-mechanical energy conversion was around 0.7×10^{-4}.

Under similar experimental conditions, a few layers of graphene decorated with gold nanoparticles in a more optimized device with 5 times higher optical absorption have reached an efficiency of $\sim 0.3 \times 10^{-3}$ at the fluence of 150 mJ/cm^2 [48]. The efficiency is linear with the laser fluence and proportional to the optical absorption, which suggests similar behavior in the GO [47,74]. However, the reported efficiencies (and pressure) are underestimated because the 30 MHz hydrophone does not integrate the high-frequency components, and the attenuation in water for the high-frequency components was not considered. Efficiencies of $\sim 10^{-3}$ are usually reported for layered devices made of directly grown or deposited carbon nano-absorbers such as carbon nanotubes (CNTs) [75–79], carbon black (CB), carbon nanofiber (CF), and carbon soot nanoparticles (CSNPs) [80,81], covered with PDMS; or metallic thin layers [82], array of metal nanostructures and AuNPs sandwiched with PDMS [83]. In most cases, the optical absorption was beyond 60 %, leading to a value 4 or 5 times higher than 0.7×10^{-4}. For instance, carbon soot and chromium ultrathin metal in PDMS films also generate high peak pressures, 4 MPa and 1.6 MPa, respectively, but start to deteriorate at the level of a few mJ cm^{-2} [47]. Peak pressures obtained with r-GO-Au, under this experimental condition, are higher than those of metallic structures covered with PDMS [84], and comparable with those obtained in functionalized carbon nanotubes in a polystyrene polymer matrix [85].

Despite the limitation of the measurement system, the measured spectral bandwidth of almost 25 MHz and 40 MHz at −6 dB and −20 dB is higher than in other composites made of different carbon materials, e.g. carbon black and nanofiber, measured with a similar system. For illustration purposes, in Fig. S4 the bandwidth at −6 dB is represented for r-GO-Au together with similar systems in the PDMS matrix, illuminated with a similar laser spot size. The spectral frequency, the pressure peak close to 1 MPa, and the method to overcome technological issues related to the production of r-GO-Au thermoelastic composite are relevant for non-destructive biomedical applications such as permeabilization of biological barriers and cell stimulation [13,49,50,86].

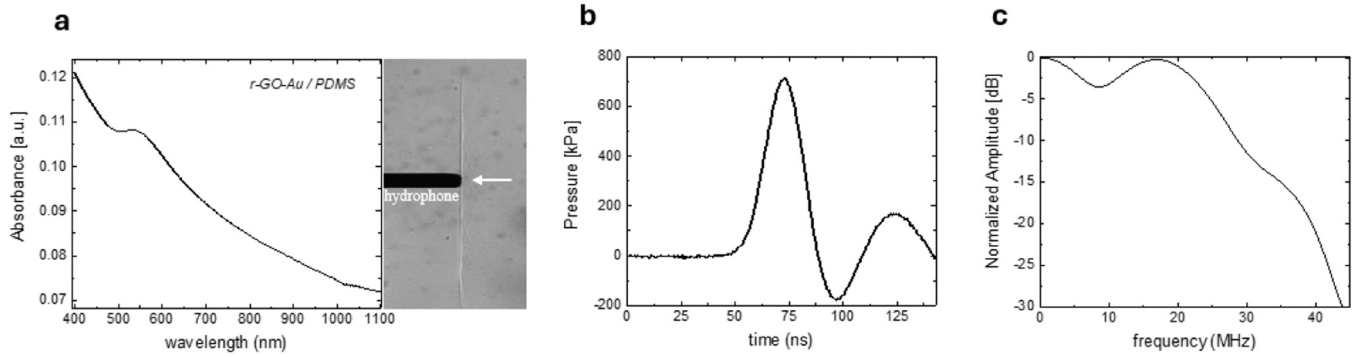

Fig. 6. (a) Absorbance of the thermoelastic film made of r-GO-AuNPs in PDMS matrix. The left panel is a shadow photograph of the propagating pressure wave, and the needle hydrophone is positioned normally to the incident wave. (b) A pressure wave signal is detected by the hydrophone and reconverted in pressure. (c) Fourier spectrum of the pressure signal is shown in (b).

4. Conclusion

In conclusion, we report on a straightforward and improved, modified bottom-up, two-step synthesis of decorated GO and r-GO. This method is both cost-effective and low in toxicity, facilitating the straightforward and reproducible fabrication of GO and r-GO, which are densely covered with Au and Pt NPs with diameters around 20 nm and 3 nm, respectively. The presented method could be easily scaled up to synthesize larger quantities of decorated graphene oxide simply by using larger volumes of dispersions and solutions at the described synthesis conditions. Another advantage of this method is the absence of a reducing agent that leads to a direct nucleation of nanoparticles only on the graphene oxide surface, and not in the solution. This enables easier isolation of decorated GO and lower consumption of noble metal complexes at the same time, and efficient decoration with negligible residual. Moreover, the reduction of GO in r-GO can be carried out in a separate step with ascorbic acid. Contrary to other reducing agents, e.g. hydrazine, the r-GO obtained from ascorbic acid presents an enhanced compatibility with organic solvents that swell Polydimethylsiloxane, and this enriches the industrial applicability. The obtained r-GO-Au solution dispersed into the PDMS was used to produce thermoelastic thin films on flexible substrates, which enables promising optoacoustic applications in biomedicine.

CRediT authorship contribution statement

Ali Rezaei: Writing – review & editing, Methodology, Investigation, Formal analysis, Data curation. **Polona Umek:** Writing – review & editing, Methodology, Investigation, Formal analysis, Data curation. **Ales Mrzel:** Writing – review & editing, Writing – original draft, Supervision, Methodology, Investigation, Formal analysis, Data curation, Conceptualization. **Matija Jezeršek:** Writing – review & editing, Funding acquisition, Formal analysis, Data curation. **Damjan Vengust:** Writing – review & editing, Methodology, Investigation, Formal analysis, Data curation. **Daniele Vella:** Writing – review & editing, Writing – original draft, Methodology, Investigation, Funding acquisition, Formal analysis, Data curation, Conceptualization.

Declaration of Competing Interest

The authors declare that they have no known competing financial interests or personal relationships that could have appeared to influence the work reported in this paper.

Acknowledgement

We acknowledge financial support through the Javna Agencija za znanstvenoraziskovalno in inovacijsko dejavnost Republike Slovenije, project no. J7-50094 (2D-Ultras), Program Group P2-0392. We acknowledge the CENN Nanocenter, and the support from the Nano-Space COST action (CA21126 – European Cooperation in Science and Technology).

Appendix A. Supporting information

Supplementary data associated with this article can be found in the online version at doi:10.1016/j.synthmet.2025.117894.

Data availability

Data will be made available on request.

References

[1] X. Fu, J. Lin, Z. Liang, R. Yao, W. Wu, Z. Fang, W. Zou, Z. Wu, H. Ning, J. Peng, Graphene oxide as a promising nanofiller for polymer composite, Surf. Interfaces 37 (2023) 102747.
[2] H. Kim, A.A. Abdala, C.W. Macosko, Graphene/polymer nanocomposites, Macromol 43 (2010) 6515–6530.
[3] J.D. Roy-Mayhew, I.A. Aksay, Graphene materials and their use in dye-sensitized solar cells, Chem. Rev. 114 (2014) 6323–6348.
[4] G. Bottari, M.Á. Herranz, L. Wibmer, M. Volland, L. Rodríguez-Pérez, D.M. Guldi, A. Hirsch, N. Martín, F. D'Souza, T. Torres, Chemical functionalization and characterization of graphene-based materials, Chem. Soc. Rev. 46 (2017) 4464–4500.
[5] Z. Sun, Z. Liu, J. Li, G. Tai, S.-P. Lau, F. Yan, Infrared photodetectors based on CVD-grown graphene and PbS quantum dots with ultrahigh responsivity, Adv. Mater. 24 (2012) 5878–5883.
[6] K.F. Mak, M.Y. Sfeir, Y. Wu, C.H. Lui, J.A. Misewich, T.F. Heinz, Measurement of the optical conductivity of graphene, Phys. Rev. Lett. 101 (2008) 196405.
[7] O.C. Compton, S.T. Nguyen, Graphene oxide, highly reduced graphene oxide, and graphene: versatile building blocks for carbon-based materials, Small 6 (2010) 711–723.
[8] C. Nethravathi, M. Rajamathi, Chemically modified graphene sheets produced by the solvothermal reduction of colloidal dispersions of graphite oxide, Carbon 46 (2008) 1994–1998.
[9] Z. Fan, K. Wang, T. Wei, J. Yan, L. Song, B. Shao, An environmentally friendly and efficient route for the reduction of graphene oxide by aluminum powder, Carbon 48 (2010) 1686–1689.
[10] S. Park, R.S. Ruoff, Chemical methods for the production of graphenes, Nat. Nanotechnol. 4 (2009) 217–224.
[11] G. Wang, J. Yang, J. Park, X. Gou, B. Wang, H. Liu, J. Yao, Facile synthesis and characterization of graphene nanosheets, J. Phys. Chem. C 112 (2008) 8192–8195.
[12] S. Pei, J. Zhao, J. Du, W. Ren, H.-M. Cheng, Direct reduction of graphene oxide films into highly conductive and flexible graphene films by hydrohalic acids, Carbon 48 (2010) 4466–4474.
[13] J. Zhang, H. Yang, G. Shen, P. Cheng, J. Zhang, S. Guo, Reduction of graphene oxide via L-ascorbic acid, Chem. Commun. 46 (2010) 1112–1114.
[14] S. Bose, T. Kuila, A.K. Mishra, N.H. Kim, J.H. Lee, Dual role of glycine as a chemical functionalizer and a reducing agent in the preparation of graphene: an environmentally friendly method, J. Mater. Chem. 22 (2012) 9696–9703.
[15] C. Zhu, S. Guo, Y. Fang, S. Dong, Reducing sugar: new functional molecules for the green synthesis of graphene nanosheets, ACS Nano 4 (2010) 2429–2437.
[16] A. Esfandiar, O. Akhavan, A. Irajizad, Melatonin as a powerful bio-antioxidant for reduction of graphene oxide, J. Mater. Chem. 21 (2011) 10907–10914.

[17] Y. Liu, R. Cheng, L. Liao, H. Zhou, J. Bai, G. Liu, L. Liu, Y. Huang, X. Duan, Plasmon resonance enhanced multicolour photodetection by graphene, Nat. Commun. 2 (2011) 579.

[18] T.J. Echtermeyer, L. Britnell, P.K. Jasnos, A. Lombardo, R.V. Gorbachev, A. N. Grigorenko, A.K. Geim, A.C. Ferrari, K.S. Novoselov, Strong plasmonic enhancement of photovoltage in graphene, Nat. Commun. 2 (2011) 458.

[19] S. Li, X. Jin, Y. Shao, X. Qi, J. Yang, Y. Wang, Gold nanoparticle/reduced graphene oxide hybrids for fast light-actuated shape memory polymers with enhanced photothermal conversion and mechanical stiffness, Eur. Polym. J. 116 (2019) 302–310.

[20] D.O. Idisi, E.M. Benecha, S.J. Moloi, S.C. Ray, Effects of gold nanoparticles (Au-NPs) on the electrical properties of reduced graphene oxide: an experimental and DFT study, J. Mater. Res. 37 (2022) 1037–1046.

[21] X. Dong, W. Huang, P. Chen, In situ synthesis of reduced graphene oxide and gold nanocomposites for nanoelectronics and biosensing, Nanoscale Res. Lett. 6 (2010) 60.

[22] W. Niu, H. Chen, R. Chen, J. Huang, A. Palaniappan, H. Sun, B.G. Liedberg, A.I. Y. Tok, Synergetically enhanced near-infrared photoresponse of reduced graphene oxide by upconversion and gold plasmon, Small 10 (2014) 3637–3643.

[23] M.L. Yola, N. Atar, T. Eren, H. Karimi-Maleh, S. Wang, Sensitive and selective determination of aqueous triclosan based on gold nanoparticles on polyoxometalate/reduced graphene oxide nanohybrid, RSC Adv. 5 (2015) 65953–65962.

[24] A. Marinoiu, E. Carcadea, A. Sacca, A. Carbone, C. Sisu, A. Dogaru, M. Raceanu, M. Varlam, One-step synthesis of graphene supported platinum nanoparticles as electrocatalyst for PEM fuel cells, Int. J. Hydrog. Energy 46 (2021) 12242–12253.

[25] I. Khalil, N.M. Julkapli, W.A. Yehye, W.J. Basirun, S.K. Bhargava, Graphene-gold nanoparticles hybrid—synthesis, functionalization, and application in a electrochemical and surface-enhanced Raman scattering biosensor, Materials 9 (2016) 406.

[26] M. Faraday, X. the bakerian lecture. —experimental relations of gold (and other metals) to light, Philos. Trans. R. Soc. Lond. 147 (1857) 145–181.

[27] C.D. Bain, E.B. Troughton, Y.T. Tao, J. Evall, G.M. Whitesides, R.G. Nuzzo, Formation of monolayer films by the spontaneous assembly of organic thiols from solution onto gold, J. Am. Chem. Soc. 111 (1989) 321–335.

[28] T. Bürgi, Properties of the gold–sulphur interface: from self-assembled monolayers to clusters, Nanoscale 7 (2015) 15553–15567.

[29] R. Karthik, M. Govindasamy, S.-M. Chen, V. Mani, B.-S. Lou, R. Devasenathipathy, Y.-S. Hou, A. Elangovan, Green synthesized gold nanoparticles decorated graphene oxide for sensitive determination of chloramphenicol in milk, powdered milk, honey and eye drops, J. Colloid Interface Sci. 475 (2016) 46–56.

[30] M.N.I. Amir, A. Halilu, N.M. Julkapli, A. Ma'amor, Gold-graphene oxide nanohybrids: a review on their chemical catalysis, J. Ind. Eng. Chem. 83 (2020) 1–13.

[31] L. Shao, X. Huang, D. Teschner, W. Zhang, Gold supported on graphene oxide: an active and selective catalyst for phenylacetylene hydrogenations at low temperatures, ACS Catal. 4 (2014) 2369–2373.

[32] H. Yang, W. Zhou, B. Yu, Y. Wang, C. Cong, T. Yu, Uniform decoration of reduced graphene oxide sheets with gold nanoparticles, J. Nanotechnol. 2012 (2012) 328565.

[33] S. Rattan, S. Kumar, J.K. Goswamy, Gold nanoparticle decorated graphene for efficient sensing of NO2 gas, Sens. Int. 3 (2022) 100147.

[34] Z. Zhang, H. Chen, C. Xing, M. Guo, F. Xu, X. Wang, H.J. Gruber, B. Zhang, J. Tang, Sodium citrate: a universal reducing agent for reduction/decoration of graphene oxide with Au nanoparticles, Nano Res. 4 (2011) 599–611.

[35] S. Bai, X. Shen, Graphene–inorganic nanocomposites, RSC Adv. 2 (2011) 64–98.

[36] B. Munkhbayar, Md.J. Nine, S. Hwang, J. Kim, K. Bae, H. Chung, H. Jeong, Effect of grinding speed changes on dispersibility of the treated multi-walled carbon nanotubes in aqueous solution and its thermal characteristics, Chem. Eng. Process. Process. Intensif. 61 (2012) 36–41.

[37] N. Zhang, H. Qiu, Y. Liu, W. Wang, Y. Li, X. Wang, J. Gao, Fabrication of gold nanoparticle/graphene oxide nanocomposites and their excellent catalytic performance, J. Mater. Chem. 21 (2011) 11080–11083.

[38] X. Zhang, W. Ooki, Y.R. Kosaka, A. Okonogi, G. Marzun, P. Wagener, S. Barcikowski, T. Kondo, J. Nakamura, Effect of pH on the spontaneous synthesis of palladium nanoparticles on reduced graphene oxide, Appl. Surf. Sci. 389 (2016) 911–915.

[39] F. Li, X. Gao, Q. Xue, S. Li, Y. Chen, J.-M. Lee, Reduced graphene oxide supported platinum nanocubes composites: one-pot hydrothermal synthesis and enhanced catalytic activity, J. Nanotechnol. 26 (2015) 065603.

[40] R. Nie, J. Wang, L. Wang, Y. Qin, P. Chen, Z. Hou, Platinum supported on reduced graphene oxide as a catalyst for hydrogenation of nitroarenes, Carbon 50 (2012) 586–596.

[41] P.K. Sahoo, S. Sahoo, A.K. Satpati, D. Bahadur, Solvothermal synthesis of reduced graphene oxide/Au nanocomposite-modified electrode for the determination of inorganic mercury and electrochemical oxidation of toxic phenolic compounds, Electrochim. Acta 180 (2015) 1023–1032.

[42] A. Oubraham, D. Ion-Ebrasu, F. Vasut, A. Soare, I.-S. Sorlei, A. Marinoiu, Platinum-functionalized graphene oxide: one-pot synthesis and application as an electrocatalyst, J. Mater. 16 (2023) 1897.

[43] S. Wu, J. Liu, D. Liang, H. Sun, Y. Ye, Z. Tian, C. Liang, Photo-excited in situ loading of Pt clusters onto rGO immobilized SnO2 with excellent catalytic performance toward methanol oxidation, Nano Energy 26 (2016) 699–707.

[44] E. Antolini, Graphene as a new carbon support for low-temperature fuel cell catalysts, Appl. Catal. B Environ. 123–124 (2012) 52–68.

[45] L. Zhu, X. Guo, Y. Chen, Z. Chen, Y. Lan, Y. Hong, W. Lan, Graphene oxide composite membranes for water purification, ACS Appl. Nano Mater. 5 (2022) 3643–3653.

[46] V.V. Neklyudov, N.R. Khafizov, I.A. Sedov, A.M. Dimiev, New insights into the solubility of graphene oxide in water and alcohols, Phys. Chem. Chem. Phys. 19 (2017) 17000–17008.

[47] D. Vella, A. Mrzel, A. Drnovšek, V. Shvalya, M. Jezeršek, Ultrasonic photoacoustic emitter of graphene-nanocomposites film on a flexible substrate, Photoacoustics 28 (2022) 100413.

[48] D. Vella, D.A. Pereira, A. Mrzel, D. Vengust, A. Drnovšek, L.G. Arnaut, C. Serpa, M. Jezeršek, Picosecond photoacoustic generation of ultrasounds with composites of graphene-decorated gold nanoparticles, Nano Energy 131 (2024) 110236.

[49] D.A. Pereira, A.D. Silva, P.A.T. Martins, A.P. Piedade, D. Martynowych, D. Veysset, M.J. Moreno, C. Serpa, K.A. Nelson, L.G. Arnaut, Imaging of photoacoustic-mediated permeabilization of giant unilamellar vesicles (GUVs), Sci. Rep. 11 (2021) 1–12.

[50] A.D. Silva, C. Serpa, L.G. Arnaut, Photoacoustic transfection of DNA encoding GFP, Sci. Rep. 9 (2019) 1–10.

[51] C.S. Lobo, M.I.P. Mendes, D.A. Pereira, L.C. Gomes-da-Silva, L.G. Arnaut, Photodynamic therapy changes tumour immunogenicity and promotes immune-checkpoint blockade response, particularly when combined with micromechanical priming, Sci. Rep. 13 (2023) 11667.

[52] R.J. Colchester, E.Z. Zhang, C.A. Mosse, P.C. Beard, I. Papakonstantinou, A. E. Desjardins, Broadband miniature optical ultrasound probe for high resolution vascular tissue imaging, Biomed. Opt. Express 6 (2015) 1502–1511.

[53] A. Mrzel, D. Vella, M. Jezeršek, Preparation process of graphene dispersion in PDMS with the simultaneous use of ultrasound and vacuum, EP4282905A1, Eur. Pat. (2023). EP4282905A1.

[54] P.N. Njoki, I.-I.S. Lim, D. Mott, H.-Y. Park, B. Khan, S. Mishra, R. Sujakumar, J. Luo, C.-J. Zhong, Size correlation of optical and spectroscopic properties for gold nanoparticles, J. Phys. Chem. C. 111 (2007) 14664–14669.

[55] E. Gharibshahi, E. Saion, Influence of dose on particle size and optical properties of colloidal platinum nanoparticles, Int. J. Mol. Sci. 13 (2012) 14723–14741.

[56] S.V. Otari, M. Kumar, M.Z. Anwar, N.D. Thorat, S.K.S. Patel, D. Lee, J.H. Lee, J.-K. Lee, Y.C. Kang, L. Zhang, Rapid synthesis and decoration of reduced graphene oxide with gold nanoparticles by thermostable peptides for memory device and photothermal applications, Sci. Rep. 7 (2017) 10980.

[57] H.C. Choi, M. Shim, S. Bangsaruntip, H. Dai, Spontaneous reduction of metal ions on the sidewalls of carbon nanotubes, J. Am. Chem. Soc. 124 (2002) 9058–9059.

[58] A. Kovič, A. Mrzel, J. Ravnik, S. Šturm, M. Vilfan, Surface decoration of MoSI nanowires and MoS2 multi-wall nanotubes and platinum nanoparticle encapsulation, Mater. Lett. 159 (2015) 333–336.

[59] S. Vallejos, P. Umek, T. Stoycheva, F. Annanouch, E. Llobet, X. Correig, P. De Marco, C. Bittencourt, C. Blackman, Single-step deposition of Au- and Pt-nanoparticle-functionalized tungsten oxide nanoneedles synthesized via aerosol-assisted CVD, and used for fabrication of selective gas microsensor arrays, Adv. Funct. Mater. 23 (2013) 1313–1322.

[60] X. Chen, G. Wu, J. Chen, X. Chen, Z. Xie, X. Wang, Synthesis of "clean" and well-dispersive Pd nanoparticles with excellent electrocatalytic property on graphene oxide, J. Am. Chem. Soc. 133 (2011) 3693–3695.

[61] F. Li, Y. Guo, R. Li, F. Wu, Y. Liu, X. Sun, C. Li, W. Wang, J. Gao, A facile method to synthesize supported Pd–Au nanoparticles using graphene oxide as the reductant and their extremely high electrocatalytic activity for the electrooxidation of methanol and ethanol, J. Mater. Chem. A 1 (2013) 6579–6587.

[62] M. Palomba, G. Carotenuto, A. Longo, A brief review: the use of L-ascorbic acid as a green reducing agent of graphene oxide, J. Mater. 15 (2022) 6456.

[63] U. Kanta, V. Thongpool, W. Sangkhun, N. Wongyao, J. Wootthikanokkhan, Preparations, characterizations, and a comparative study on photovoltaic performance of two different types of graphene/TiO2 nanocomposites photoelectrodes, J. Nanomater. 2017 (2017) 2758294.

[64] F. Tuinstra, J.L. Koenig, Raman spectrum of graphite, J. Chem. Phys. 53 (1970) 1126–1130.

[65] A.C. Ferrari, J.C. Meyer, V. Scardaci, C. Casiraghi, M. Lazzeri, F. Mauri, S. Piscanec, D. Jiang, K.S. Novoselov, S. Roth, A.K. Geim, Raman spectrum of graphene and graphene layers, Phys. Rev. Lett. 97 (2006) 187401.

[66] V. Scardaci, G. Compagnini, Raman spectroscopy investigation of graphene oxide reduction by laser scribing, C 7 (2021) 48.

[67] S. Claramunt, A. Varea, D. López-Díaz, M.M. Velázquez, A. Cornet, A. Cirera, The importance of interbands on the interpretation of the Raman spectrum of graphene oxide, J. Phys. Chem. C. 119 (2015) 10123–10129.

[68] A. Sadezky, H. Muckenhuber, H. Grothe, R. Niessner, U. Pöschl, Raman microspectroscopy of soot and related carbonaceous materials: spectral analysis and structural information, Carbon 43 (2005) 1731–1742.

[69] S. Vollebregt, R. Ishihara, F.D. Tichelaar, Y. Hou, C.I.M. Beenakker, Influence of the growth temperature on the first and second-order Raman band ratios and widths of carbon nanotubes and fibers, Carbon 50 (2012) 3542–3554.

[70] X. Zhao, Y. Ando, Raman spectra and X-ray diffraction patterns of carbon nanotubes prepared by hydrogen arc discharge, Jpn. J. Appl. Phys. 37 (1998) 4846.

[71] J.N. Lee, C. Park, G.M. Whitesides, Solvent compatibility of poly (dimethylsiloxane)-based microfluidic devices, Anal. Chem. 75 (2003) 6544–6554.

[72] D. Konios, M.M. Stylianakis, E. Stratakis, E. Kymakis, Dispersion behaviour of graphene oxide and reduced graphene oxide, J. Colloid Interface Sci. 430 (2014) 108–112.

[73] X. Du, J. Li, G. Niu, J.H. Yuan, K.H. Xue, M. Xia, W. Pan, X. Yang, B. Zhu, J. Tang, Lead halide perovskite for efficient optoacoustic conversion and application toward high-resolution ultrasound imaging, Nat. Commun. 12 (2021) 1–9.
[74] T. Lee, H.W. Baac, Q. Li, L.J. Guo, Efficient photoacoustic conversion in optical nanomaterials and composites, Adv. Opt. Mater. 6 (2018) 1800491.
[75] Z. Chen, Y. Wu, Y. Yang, J. Li, B. Xie, X. Li, S. Lei, J. Ou-Yang, X. Yang, Q. Zhou, B. Zhu, Multilayered carbon nanotube yarn based optoacoustic transducer with high energy conversion efficiency for ultrasound application, Nano Energy 46 (2018) 314–321.
[76] H.Won Baac, J.G. Ok, H.J. Park, T. Ling, S.L. Chen, A.J. Hart, L.J. Guo, Carbon nanotube composite optoacoustic transmitters for strong and high frequency ultrasound generation, Appl. Phys. Lett. 97 (2010) 234104.
[77] H.W. Baac, J.G. Ok, T. Lee, L. Jay Guo, Nano-structural characteristics of carbon nanotube-polymer composite films for high-amplitude optoacoustic generation, Nanoscale 7 (2015) 14460–14468.
[78] R.J. Colchester, C.A. Mosse, D.S. Bhachu, J.C. Bear, C.J. Carmalt, I.P. Parkin, B. E. Treeby, I. Papakonstantinou, A.E. Desjardins, Laser-generated ultrasound with optical fibres using functionalised carbon nanotube composite coatings, Appl. Phys. Lett. 104 (2014) 173502.
[79] S. Noimark, R.J. Colchester, R.K. Poduval, E. Maneas, E.J. Alles, T. Zhao, E. Z. Zhang, M. Ashworth, E. Tsolaki, A.H. Chester, N. Latif, S. Bertazzo, A.L. David, S. Ourselin, P.C. Beard, I.P. Parkin, I. Papakonstantinou, A.E. Desjardins, Polydimethylsiloxane composites for optical ultrasound generation and multimodality imaging, Adv. Funct. Mater. 28 (2018) 1704919.
[80] B.Y. Hsieh, J. Kim, J. Zhu, S. Li, X. Zhang, X. Jiang, A laser ultrasound transducer using carbon nanofibers–polydimethylsiloxane composite thin film, Appl. Phys. Lett. 106 (2015) 021902.
[81] W.Y. Chang, W. Huang, J. Kim, S. Li, X. Jiang, Candle soot nanoparticles-polydimethylsiloxane composites for laser ultrasound transducers, Appl. Phys. Lett. 107 (2015) 161903.
[82] T. Lee, L.J. Guo, Highly efficient photoacoustic conversion by facilitated heat transfer in ultrathin metal film sandwiched by polymer layers, Adv. Opt. Mater. 5 (2017) 1–9.
[83] X. Zou, N. Wu, Y. Tian, X. Wang, Broadband miniature fiber optic ultrasound generator, Opt. Express 22 (2014) 18119–18127.
[84] Y. Hou, J.S. Kim, S. Ashkenazi, M. O'Donnell, L.J. Guo, Optical generation of high frequency ultrasound using two-dimensional gold nanostructure, Appl. Phys. Lett. 89 (2006) 093901.
[85] A.D. Silva, C.A. Henriques, D.V. Malva, M.J.F. Calvete, M.M. Pereira, C. Serpa, L. G. Arnaut, Photoacoustic generation of intense and broadband ultrasound pulses with functionalized carbon nanotubes, Nanoscale 12 (2020) 20831–20839.
[86] Z. Du, M. Li, G. Chen, M. Xiang, D. Jia, J.-X. Cheng, C. Yang, Mid-infrared photoacoustic stimulation of neurons through vibrational excitation in polydimethylsiloxane, Adv. Sci. 11 (2024) 2405677.